Δελτίο της Ελληνικής Γεωλογικής Εταιρίας, Τομ. XXXIV/5, 2033-2038, 2001 Bulletin of the Geological Society of Greece, Vol. XXXIV/5, 2033-2038, 2001
Πρακτικά 9ου Διεθνούς Συνεδρίου, Αθήνα, Σεπτέμβριος 2001 Proceedings of the 9th International Congress, Athens, September 2001

COMPUTER TECHNIQUES FOR IMAGING EARTHQUAKE DEFORMATION USING SATELLITE DATA AND DIGITAL ELEVATION MODELS.

A. GANAS[1], E. LAGIOS[2], G. STAVRAKAKIS[1]

ABSTRACT

Earthquake deformation comprises both instantaneous, co-seismic strain and cumulative deformation over several earthquake cycles. Co-seismic deformation following events greater than 6-6.5 Ms is mapped using differential interferometry and possibly images from the new generation, very-high spatial resolution sensors. Cumulative deformation is mapped using photo/image-interpretation techniques on enhanced satellite data, both optical and radar. If strain markers can be identified on satellite imagery such as displaced channels, then some of the kinematics of deformation (slip direction, amount) can be extracted. Remote sensing can also provide conclusive evidence towards identifying the surface expression of seismogenic structures during events between 5.5 and 6 Ms.

KEY WORDS: EARTHQUAKES, SAR INTERFEROMETRY, REMOTE SENSING, DEM, ATTICA.

INTRODUCTION

The use of spaceborne images in active fault mapping is a well-established technique because they provide digital views of the earth's surface (Armijo et al., 1986; 1999; Ganas et al., 1998, 2001; Figure 1). These images are two-dimensional, digital recordings of the Earth-leaving radiance ($W/m^2 \cdot sr^{-1}$) from satellites orbiting the planet at distances between 400 and 900 km. The "system" of observation is well established, with both the illuminating source (sun) and orbital height being stable and sensor performance relatively stable over time. A popular use of optical Earth-Observation (EO) data is to map long-term neotectonic deformation (hundreds up to several millions of years). For example, Landsat TM data processing has been an effective tool for recognising large landforms (alluvial fans, transverse bedrock ridges, "wine-glass" valleys) indicative of neotectonic faulting (Figure 1). The recognition of these features is based on their geometry (e.g. arcuate shape for fans, axial drainage for rivers). In all cases, mapping follows data import, geometric and radiometric corrections, image enhancements, high-pass filtering, and other digital procedures (see Mather, 1987, pages 112-275).

The second important parameter in mapping ground deformation is relief. Topography has been modeled as a proxy for fault displacement (Anders and Schlische, 1994). Digital Elevation Models (DEMs) are raster analogs of topography originating mainly from photogrammetry (at visible wavelengths) and radargrammetry (airborne-spaceborne C-band data). During the 1990's across-track, monochromatic data such as SPOT 1A, ERS Precision PRI, ERS Single Look Complex SLCi and RADARSAT fine beam data were used to extract relatively accurate (10-20 m z-RMSe; Giles and Franklin, 1996; Krupnik, A., 2000) DEMs after applying automated stereomatching procedures. The DEMs are mainly used in mapping fault segment boundaries within rift systems because the latter are assumed to coincide with low footwall elevations, and in 2-pass, interferometric SAR processing studies to subtract the topographic phase. Since early 2000 the availability of IKONOS type data imply that depending on the quality of the exterior orientation, difference DEMs could be computed to yield a large (≥ 7 Ms) earthquake deformation map. The IKONOS DEMs accuracy varies between 1-3 metres, however, this is still under investigation due to orbital data restrictions from the US company that operates the satellite.

METHODS FOR EARTHQUAKE DEFORMATION IMAGING

Optical data

A useful method to visualize a seismogenic fault is to apply digital processing techniques to obtain either

1. Geodynamics Institute, National Observatory of Athens, P.O. BOX 20048, Athens 11810, Greece, E-mail: aganas@gein.noa.gr
2. Department of Geophysics, University of Athens, 157 84 Athens, Greece.

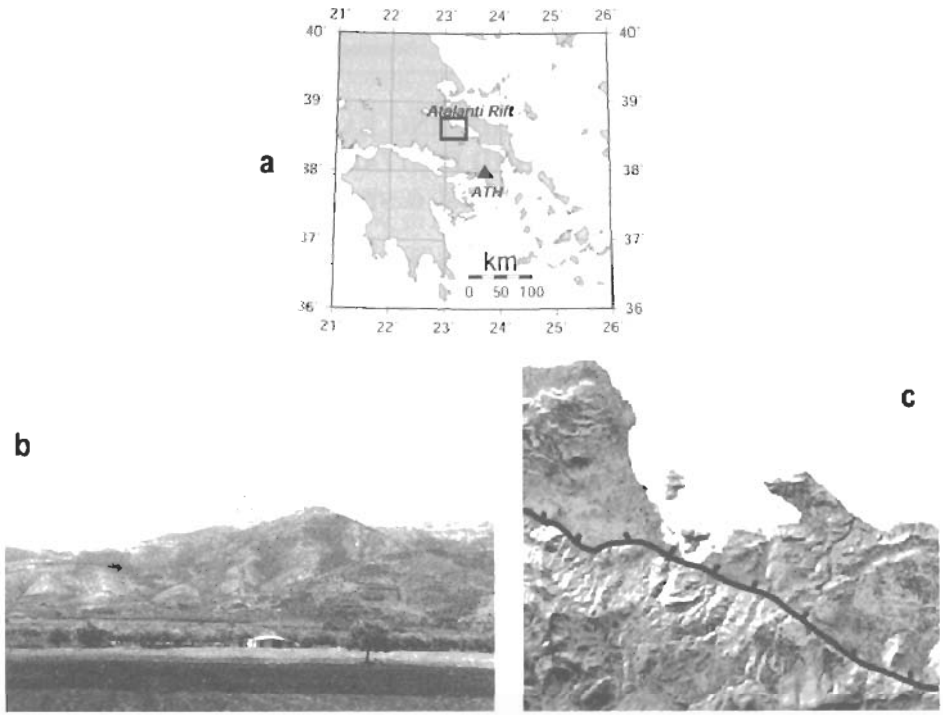

Figure 1. Images of the active Atalanti fault segment, central Greece after Ganas et al., (1998). a): Location map b) Field photograph normal to strike (look to southwest) showing wine-glass valleys terminating abruptly at the fault line c) Landsat 4 TM satellite image of January 1988, band 5 (mid-infrared). The fault runs diagonally NW-SE. The image look-up-table has been inverted to show geological structure more clearly (shadowed areas are shown as bright). Point A is the top of Chlomon Mountain (1079 m).

nadir or oblique, panoramic views of the greater area it deforms. The views help to

1. Map the extent of the structure and measure its length (Figure 1). This is helpful to estimate various seismic parameters, such rupture length and associated maximum magnitude etc
2. Estimate cumulative offset along strike by identifying displaced ridges. This is used to estimate horizontal strain and amount of extension by assuming a fixed angle of slip
3. To identify cross faults and
4. To study the long-term evolution of landforms in the meisoseismal area of a large earthquake. This can be done by calculating geomorphic ratios, such as sinuosity indices, valley widths to valley lengths ratios etc.

In nadir views of satellite data shaded relief images can be produced by choosing various illumination conditions to examine the landform pattern. The long-term evolution is assumed to result from accumulated coseismic motions (uplift-subsidence) and erosion due to climatic variations. An example is given in the shaded relief image of Figure 2b, that simulates a low sun angle (zenith=75°), southeastern viewing direction (140° N) of the western Attica region in Greece. This image is effectively a DEM of cartographic origin (HAGS, 1992) that can be used as a raster background to overlay vector files like the shallow aftershock sequence of the 7/9/1999 Ms 5.9 earthquake (Pavlides et al., 1999; Papadopoulos et al., 2000). A southeastern illumination accentuates topography better because in central Greece the predominant extension direction is north south Clarke et al., 1998). The same image can also host damage information after the collection of field observations and other macroseismic data (Ganas et al., 2001).

Oblique views are constructed to visualize the pattern of regional structures (Figure 2a) in the vicinity of the epicentre of an earthquake. Here a technique called "draping" is applied, where a colour composite, satellite image of comparable pixel size to a pre-existing DEM is overlain. The resulting file can be rotated to a variety of viewing directions to enable the geologist to make better observations of the fault pattern. An exaggeration of the topography is necessary to distinguish fault segmentation associated with slip deficits and low relief. In the

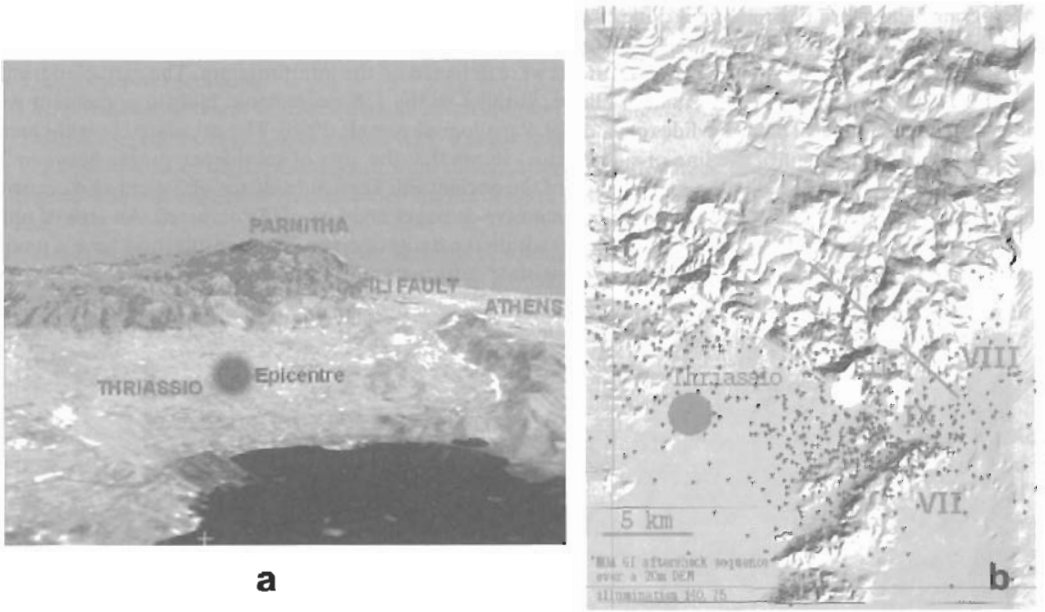

Figure 2a) Perspective view (towards northeast at 35° above the horizon) of western Attica, Greece. The image was constructed using computer vision techniques, TM imagery (741 RGB) and a 20-m DEM. Dark gray line is the trace of the Fili normal fault that moved during the 7/9/1999 earthquake. Vertical exaggeration x 3. 2b) Shaded relief image of a Digital Elevation model of the meisoseismal area simulating orientation of topography with respect to an illumination source (SE-140; zenith angle of 75 degrees). Light gray line is the Thriassion normal fault; gray line is the Fili normal fault. Crosses are aftershock epicentres; Gray circle is the relocated NOAGI epicentre of the main shock of Sept. 7, 1999. Map shows also the distribution of rock falls (white circles). Roman capital letters indicate the earthquake intensity.

case of Figure 2a fault segment boundaries may be identified on both ends of the Thriassion normal fault segment, and on the eastern end of the Fili normal fault segment in Attica, Greece. A vector layer, the trace of the Fili fault (dark gray line), is also superimposed to show the exact location of the seismogenic structure. To accurately register DEMs and Landsat, SPOT, or ASTER satellite data we need suitable grid spacing of the order of 10-to-20-m. The most accurate DEMs are produced by on-screen digitising of elevation contours of the 1:50,000 map sheets (contour interval 20 m). The degree of co-registration needs to be better than one pixel of the satellite image.

Radar data

The Interferometry technique (InSAR) was applied to study the earthquake behaviour of active faults in various parts of the world including Greece (Massonnet et al., 1993; Meyer et al., 1996; Wright et al., 1999, Kontoes et al., 2000, see Figure 3). This mapping capability is possible on regional and even global scales using specialized, radar processing software. Digital Elevation Models (DEMs) may be also created with height accuracies on the order of 5-20 metres. Detailed analysis of the phase part of the signal along the line of sight can determine the surface displacement that has occurred between successive orbits of the satellite, even when the orbits are years apart. However, the technique works much better in flat and dry areas because of constraints in the imaging geometry (the ERS satellite has a high incidence angle, 23°) and the climatic influence on phase coherence since wet climatic conditions cause quick, temporal decorrelation of the phase returns.

In this study we used the ATLANTIS software for Windows NT (version 1.2.1) where the 2-pass digital processing procedure (Figure 3) involves a) resampling of the 20-m, external DEM to the master SAR image (orbit 23136 – 23 September 1999), b) distortion of the re-sampled DEM creating foreshortening and layover distortions c) fine, interactive co-registration of the DEM to the master SAR image using more than 20 tie points with residuals less than a pixel d) calculation and subtraction of the topographic phase from the

interferogram. The phase unwrapping is done by the use of the iterative disk-masking algorithm with controlled error propagation and error correction. The algorithm uses multiple tiling and seeding techniques. Neither remaining topographic phase nor atmospheric effects were detected on the interferogram. The extracted fringes show an N110-N120 axis of the deformation ellipse, parallel to the Fili neotectonic fault in agreement with geological and seismological data (Pavlides et al., 1999, Papadopoulos et al., 2000). The calculated height-change map (the vertical component of the line-of-sight vector) shows that the area of subsidence ranges between 2-7 cm with the maximum observed in the greater area of the ancient Fili Fort. Subsidence of 2-4 cm also occurred in the Ano Liossia Area of the Athens basin where extensive damages and loss of life occurred. An area of uplift at the bottom centre is so marginal (3-8 mm) that lies within the limits of error. These results may have a unique value because no GPS data exist to measure the co-seismic deformation of the Athens earthquake.

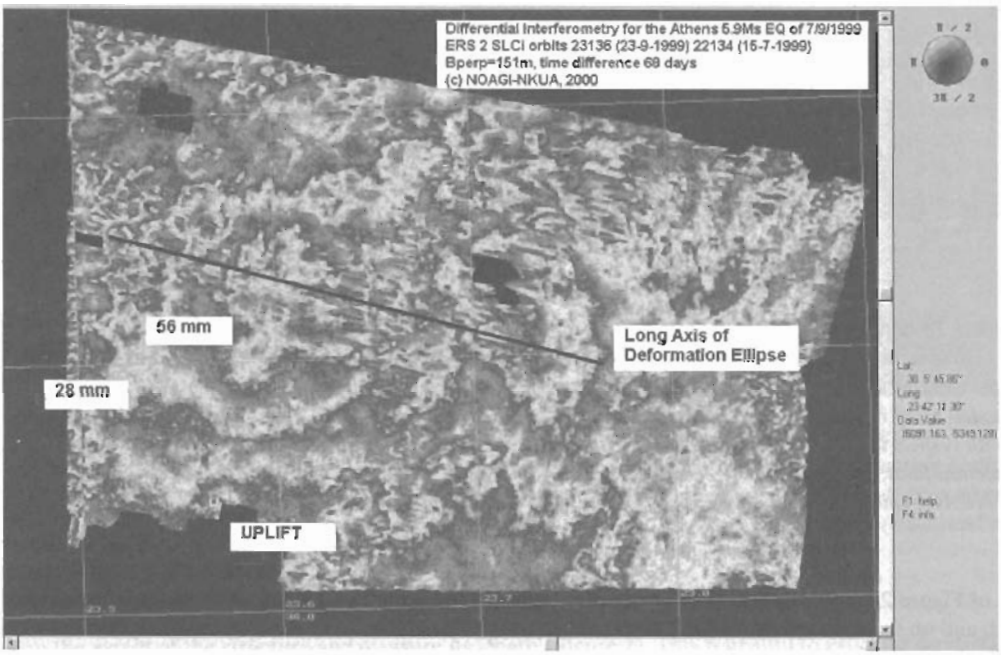

***Figure 3.** Image showing the interferogram of the Athens earthquake from the phase difference of two ERS 2 satellite images. Time difference is 68 days and the perpendicular baseline between the two orbits is 151 metres. An external digital elevation model with 20-m resolution was used to subtract pre-existing topography. Two elliptical fringes can be distinguished; the internal one labeled 56 mm, while the external 28 mm. Figures are amounts of subsidence. Black patches are areas of low coherence.*

DISCUSSION-CONCLUSIONS

Earth Observation data is another tool for the geologist/geophysicist to observe, map, display and understand the deformation pattern following large earthquakes. In particular, surface ruptures, fault scarps, landslides and ground shaking phenomena (liquefaction, slumping) following events > 7 Ms can be mapped from space using SAR Interferograms or panchromatic data from the IKONOS-2 (1 m pixel size) – IRS 1C/D (5.8 m) and SPOT-4 (10 m) satellite series. These images can be georeferenced to national grids with sub-pixel accuracy using mobile GPS networks. The mapping of surface ruptures on such large scales can supply spatial information on previously undetected active faults or small branches of large, active faults and on fault segmentation patterns if long (> 30 km) active faults have not ruptured during the last thousand years. In addition, differential Interferometry can provide 1:50000 scale maps of the full, coseismic deformation field for events exceeding 5.8 Ms.

Furthermore, remote sensing can provide conclusive evidence towards identifying the surface expression of seismogenic structures during events in the range 5.5 to 6 Ms. Because of the limited appearance or even non-existence of primary effects of the earthquake (e.g., surface ruptures) during many of the above events, data

spatial resolution and sun angle are the dominant factors that influence mapping quality.

The proposed method is:

1. The extraction of linear features (candidate structures) after digital processing of high resolution (Landsat TM/ETM+, SPOT Pan/XS/XI – IKONOS) images (Figure 1),
2. The application of digital overlays of field observations and aftershock distribution patterns on either enhanced satellite images or shaded relief images (Figure 2) to study the spatial distribution of these datasets, and
3. Comparison of the imaged faults with fault plane solutions from instrumental data and dominant slip direction in fault striation populations (e.g. Ganas et al., 2001).

This methodology can be effective even in cases where the candidate structures are spaced less than 10 km apart.

ACKNOWLEDGEMENTS

We thank Tim Wright, Xaris Kontoes, Spyros Pavlides, Gerassimos Papadopoulos, Gerald Roberts, Kevin White, Martha Stefouli, Isaak Parcharidis, Pepi Vasilopoulou, Vassilis Sakkas, Vassilis Karastathis and the ATLANTIS support team for discussions and comments. Spyros Pavlides reviewed an earlier version of the manuscript. IIS SA provided TM images and the EASI PACE software for the production of Figure 2. This work was partially funded by the GEOWARN project (IST 1999-12310).

REFERENCES

ANDERS, M. H., AND SCHLISCHE, R. W., 1994. Overlapping faults, intrabasin highs, and the growth of normal faults. *Journal of Geology*, 102, 165-180.

ARMIJO, R., TAPPONIER, P., MERCIER, J. L., AND TONG-LIN, H., 1986. Late Cenozoic right-lateral strike-slip faulting in southern Tibet: Field observations and tectonic implications. *Journal of Geophysical Research*, 91(B14), 13803-13872.

ARMIJO, R., MEYER, B., HUBERT, A., AND BARKA, A., 1999. Westward propagation of the North Anatolian fault into the northern Aegean: timing and kinematics. *Geology*, 27(3), 267-270.

CLARKE, P. J., DAVIES, R. R., ENGLAND, P. C., PARSONS, B., BILLIRIS, H., PARADISSIS, D., VEIS, G., CROSS, P. A., DENYS, P. H., ASHKENAZI, V., BINGLEY, R., KAHLE, H. G., MULLER, M. V., AND BRIOLE, P., 1998. Crustal strain in central Greece from repeated GPS measurements in the interval 1989-1997. *Geophysical Journal International*, 135, 195-214.

GANAS, A., PAPADOPOULOS, G., AND PAVLIDES, S. B., 2001. The 7th September 1999 Athens 5.9 Ms earthquake: remote sensing and digital elevation model inputs towards identifying the seismic fault. *International Journal of Remote Sensing*, 22 (1), 191-196.

GANAS, A., ROBERTS, G. P., AND MEMOU, TZ. 1998. Segment boundaries, the 1894 ruptures and strain patterns along the Atalanti Fault, Central Greece. *Journal of Geodynamics*, 26(2-4), 461 - 486.

GILES, P. T., AND FRANKLIN, S. E., 1996. Comparison of derivative topographic surfaces of a DEM generated from stereoscopic SPOT images with field measurements. *Photogrammetric Engineering and Remote Sensing*, 62(10), 1165 - 1171.

HELLENIC ARMY GEOGRAPHICAL SERVICE, 1992. Map Sheet "Elefsis".

KONTOES, C., ELIAS, P., SYKIOTI, O., BRIOLE, P., AND REMY, D., 2000. Displacement field and fault model for the September 7, 1999 Athens earthquake inferred from ERS2 satellite radar interferometry. Geophysical Research Letters, 27, 24, p. 3989.

KRUPNIK, A., 2000. Accuracy assessment of automatically derived digital elevation models from SPOT images. *Photogrammetric Engineering and Remote Sensing*, 66(8), 1017-1023.

MASSONNET, D., ROSSI, M., CARMONA, C., ADRAGNA, F., PELTZER, G., FEIGL, K., AND RABAUTE, T., 1993. The displacement field of the Landers earthquake mapped by radar interferometry. Nature, 364, 138-142.

MATHER, P. M., 1987. Computer Processing of Remotely Sensed Images: An introduction. John Wiley & Sons, 352p.

MEYER, B., ARMIJO, R., MASSONNET, D., DE CHABALIER, J. B., DELACOURT, C., RUEGG, J. C., ACHACHE, J., BRIOLE, P., AND PAPANASTASIOU, D., 1996. The 1995 Grevena (northern Greece) earthquake: fault model constrained with tectonic observations and SAR interferometry. *Geophysical Research*

Letters, 23, 2677-2680.

PAPADOPOULOS, G. A., DRAKATOS, G., PAPANASTASSIOU, D., KALOGERAS, I., STAVRAKAKIS, G., 2000, Preliminary results about the catastrophic earthquake of 7 September 1999 in Athens, Greece. *Seismological Research Letters*, 71, 318-329.

PAVLIDES, S., PAPADOPOULOS, G. A., AND GANAS, A., 1999. The 7th September 1999 unexpected earthquake of Athens: Preliminary results on the seismotectonic environment, 1st Conf. Advances in Natural Hazards Mitigation: Experiences from Europe and Japan, Programme-Abstracts-Reports, Athens, 3-4 November 1999, 80-85.

WRIGHT, T. J., PARSONS, B. E., JACKSON J. A., HAYNES, M., FIELDING, E. J., ENGLAND, P. C., AND CLARKE, P. J., 1999. Source parameters of the 1 October 1995 Dinar (Turkey) earthquake from SAR Interferometry and seismic bodywave modeling. *Earth and Planetary Science Letters*, 172(1-2), 23-37

ZEBKER, H. A., AND GOLDSTEIN, R. M., 1986. Topographic mapping from interferometric synthetic aperture radar observations. *Journal of Geophysical Research*, 91, 4993-4999.